PERGAMON

Electrochimica Acta 46 (2001) 3001–3013

ELECTROCHIMICA Acta

www.elsevier.nl/locate/electacta

Studies of model dependence in an ab initio approach to uncatalyzed oxygen reduction and the calculation of transfer coefficients

Titus V. Albu, Alfred B. Anderson *

Department of Chemistry, Case Western Reserve University, 10900 Euclid Avenue, Cleveland, OH 44106-7078, USA

Received 6 February 2001; received in revised form 24 March 2001

Abstract

In a recent study [J. Am. Chem. Soc. 121 (1999) 11855], an ab initio approach to calculate potential dependent activation energies was applied in studying the outer-sphere O_2 reduction and H_2O oxidation. The purpose of this paper is to examine influences of changes in the calculational methodology and the reactant structural models. The first step in the overall four-electron reduction of O_2 to water,

$$O_2(g) + H^+(aq) + e^-(U) \rightleftharpoons HOO(aq)$$

is the focus of this work. U is the electrode potential and $H^+(aq)$ is modeled by the $[HOH_2(OH_2)_2]^+$ cluster. For an electrode potential of 0.727 V on the hydrogen scale, the findings of this study are:

1. Determining the transition state structures constrained to using the product OOH angle is a satisfactory approximation.
2. The calculated activation energies are reduced for the forward reaction and increased for the reverse reaction when the hydronium ion structure is relaxed along the reaction coordinate.
3. Calculated reduction activation energies using the 6-31G** basis set are highest for the HF calculations, intermediate for MP2 calculations and lowest for B3LYP density functional calculations. Adding diffuse functions lowers all of the values.
4. Increasing the model size by coordinating another water molecule to the transferring proton increases the activation energy for the forward reaction.

In addition to the above, the transfer coefficients in the Butler–Volmer equation relating current density to overpotential are calculated and discussed.

Keywords: Theory; Oxygen reduction; Transfer coefficients

1. Introduction

Oxygen reduction is the cathodic process in fuel cells. The best-known electrocatalysts for oxygen reduction in acid electrolytes are platinum and its alloys [1]. Though potential replacements for the expensive platinum electrode, including other metals [2], oxides [3], transition metal macrocyclic complexes [4–6], and pyrolized transition metal complexes [7,8], have been investigated for a long time, a good substitute is still to be discovered. The goal is high current density at low overpotential for the four-electron reduction of oxygen to water:

* Corresponding author. Tel.: +1-216-3685044; fax: +1-216-3683006.

E-mail address: aba@po.cwru.edu (A.B. Anderson).

0013-4686/01/$ - see front matter
PII: S0013-4686(01)00515-1

$$O_2(g) + 4H^+(aq) + 4e^-(U) \rightarrow 2H_2O(l) \quad (1)$$

where U is the electrode potential. The standard reversible potential for Eq. (1) is 1.229 V on the standard hydrogen scale. Overpotentials are typically ~ 0.4 V, meaning the potential of the working electrode is $\sim$ 0.85 V. The significant issues and mechanistic aspects on the electrocatalytic oxygen reduction process are covered in recent reviews of the field [9–12]. Recently there has been an increase in theoretical activity regarding electrochemical processes involving bond breaking and forming [13,14], and electrode interfacial properties [15–17]. In this context, mechanistic aspects of the O_2 reduction over platinum [18,19], silver [20], transition metal oxides [21], and transition metal macrocyclic complexes [22] have been studied with semiempirical methods during the last decade.

This laboratory has recently been working to develop an ab initio quantum chemistry approach for studying the electrode potential dependence of electrocatalytic reactions. The model is based on the idea of radiationless electron tunneling between the electrode and the reaction center, as was first introduced by Gurney [23]. This methodology has been applied in examining hydrogen evolution from conducting diamond film cathodes [24], oxygen reduction in the outer-Helmholtz-plane region [25,26], and platinum-catalyzed oxygen reduction [27].

In the uncatalyzed oxygen reduction study [25,26], the following one-electron steps were modeled:

$$O_2(g) + H^+(aq) + e^- \rightarrow HOO^{\bullet}(aq) \quad (2)$$

$$HOO^{\bullet}(aq) + H^+(aq) + e^- \rightarrow H_2O_2(aq) \quad (3)$$

$$H_2O_2(aq) + H^+(aq) + e^- \rightarrow HO^{\bullet}(g) + H_2O(l) \quad (4)$$

$$HO^{\bullet}(g) + H^+(aq) + e^- \rightarrow H_2O(l) \quad (5)$$

It was determined that, over the considered potential range between 0 and 2 V, H_2O_2 reduction, Eq. (4), has the highest activation energy, followed by O_2 reduction, Eq. (2), while $HOO^{\bullet}$ and $HO^{\bullet}$ reduction have small activation energies. These results are consistent with the experimental observation of hydrogen peroxide generation over the weakly interacting electrodes like mercury [28] and hydrogenated platinum [29]. Calculated reduction activation energies for all four steps were found to increase as the electrode potential was increased over the potential range considered.

The same reactions where studied by this theory with the reduction intermediates bonded to platinum and the activation energies for O_2 and H_2O_2 reduction were calculated to be smaller compared with the uncatalyzed case by about 0.9 eV [27]. The catalytic effect of platinum was explained in terms of bond strength variation between platinum and the reactants, intermediates, and products.

An $H^+(aq)$ model similar to that used here was the basis of a study of proton discharge and H_2 generation on Cu(100) [30] and GaAs(111) [31,32] surfaces. In that work the electrode potential was not introduced as a parameter, the focus being on the partial electronic charge transfer concept [33].

The purpose of this article is to amplify on the model assumptions of the previous papers [25,26] dealing with the outer-Helmholtz plane of oxygen reduction and water oxidation. The present study includes finding the sensitivity of the potential dependent activation energy for the first one-electron reduction, Eq. (2), to: (i) the structure of solvated proton models; (ii) the basis set size; and (iii) the calculational method employed.

2. Theoretical method

2.1. Computational methods and basis sets

Standard ab initio and density functional theory (DFT) calculations have been carried out using the GAUSSIAN-98 suite of programs [34]. Restricted wave functions have been used for the closed-shell systems and unrestricted wave functions for open-shell systems. The methods used are Hartree–Fock (HF), Becke's three-parameter hybrid DFT method with the Lee–Yang–Parr correlation functional (B3LYP), Møller–Plesset perturbation theory for electron-correlation corrections truncated at the second order (MP2), and quadratic configuration interaction theory including single and double substitutions (QCISD). Basis set analysis has been performed with basis sets increasing in complexity starting from a simple split-valence double-ζ basis set, 6-31G, to a polarized split-valence triple-ζ augmented with diffuse functions basis set, 6-311 + G(2d,p).

2.2. Model for electrode potential and potential dependence

The chemical potential of electrons at the electrode surface is equal to the negative of the thermodynamic work function, φ, of the electrode surface. On the standard hydrogen electrochemical scale, the electrode potential $U(V)$ is given by:

$$U/V = \varphi/\text{eV} - \varphi_{H^+/H_2}/\text{eV} \quad (6)$$

where φ_{H^+/H_2} is the thermodynamic work function of the standard hydrogen electrode for which the value of 4.6 eV [35], an average of experimentally determined values, is used in this study.

The electrode, which is an electron source in reduction reactions, can be modeled by a non-interacting electron donor molecule with a chosen ionization potential (IP). The reactant that is to undergo reduction,

R^+, reaches, due to the thermal activation, a point on the reaction path where its electron affinity (EA), matches the donor IP. An electron transfer by non-radiative tunneling is then assumed to occur and the donor's IP or reaction center's EA is identified with the electrode potential U as:

$$U/V = \text{IP (donor)/eV} - 4.6$$
$$= \text{EA (reaction center)/eV} - 4.6 \quad (7)$$

The EA is calculated as the negative of the non-adiabatic electron attachment energy. For an oxidation reaction, an acceptor molecule with an adjustable EA may be used to model the electrode acting as an electron sink and, based on the same considerations as above, the electrode potential is given by:

$$U/V = \text{EA (acceptor)/eV} - 4.6$$
$$= \text{IP (reaction center)/eV} - 4.6 \quad (8)$$

The IP is calculated as the vertical ionization energy.

It is possible to eliminate the donor and acceptor species and find the transition states and their potential dependencies by a careful analysis of the potential energy surfaces of the reactant, $R^+ + e^-$, and product, R, species. This approach is used here because it avoids the computational convergence problem of the electron not always transferring from the donor molecule to the reaction center when it would be energetically preferred to do so, a situation observed in the study on hydrogen evolution from diamond electrodes [24]. Corrections for zero-point energies are not included in the present level of modeling, and for the reaction studied they nearly cancel.

3. Results and discussion

3.1. Effects of relaxing model structures constraints

The process of one-electron reduction of O_2 to HOO in acid solution requires that the reactants, oxygen and hydronium ion, to come close to each other and form a hydrogen-bonded complex, $OO\cdots H^+–OH_2(OH_2)_2$, which is referred to as the reduction precursor. The reduction activation energies are calculated with respect to the energy of this precursor. Similarly, for the reverse oxidation reaction, OO–H and $OH_2(OH_2)_2$ form a hydrogen-bonded oxidation precursor, $OO–H\cdots OH_2(OH_2)_2$. To reach the electron-transfer state, which is at higher energy, these precursors need to be thermally activated. At the electron-transfer state corresponding to a certain electrode potential, the EA of the reaction center in the oxidized form, $OO\cdots H^+\cdots OH_2(OH_2)_2$, or the IP of the reaction center in the reduced form, $OO\cdots H\cdots OH_2(OH_2)_2$, is related to the electrode potential through Eqs. (7) and (8). In this study, the electron-transfer state coincides with the transition state (TS). The identity of electron-transfer state with the TS can be understood when considering the bond order changes that occur when electron transfers and these will be discussed in detail later.

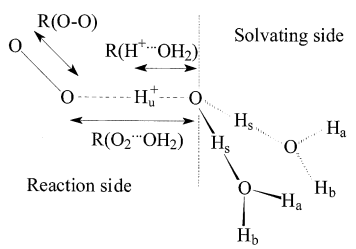

Fig. 1. Model system showing the variables optimized in determining hydrogen-bonded precursors and transition state structures for the first step in O_2 reduction. The labels a, b, s, and u are used in Table 1.

In order to simplify the calculations, the reaction coordinate and therefore hydrogen-bonded precursors and transition states are calculated with the same constraints as in the previous studies: (i) the $OH_2(OH_2)_2$ fragment of the solvated hydronium ion is kept rigid; (ii) the proton is moved along the internuclear line connecting receiving oxygen atom of O_2 and the oxygen atom of the solvated H_3O^+ so that $OO\cdots H^+\cdots OH_2(OH_2)_2$ is linear; and (iii) the O–O–H^+ angle is set equal to the value calculated for the optimized OOH product. Based on the above simplifications, the TS is determined by searching for the structures with the desired EA, in a three-dimensional (3D) space: O–O, $OO\cdots OH_2(OH_2)_2$, and $H^+\cdots OH_2(OH_2)_2$ distances, as defined in Fig. 1. A solvation structure for H_3O^+ has been chosen and because its interface with the bulk solution may have a hydrogen-bonded structure it is inappropriate to optimize the orientational angles of the two solvating water molecules. However, relaxations of the other two O–H bonds in H_3O^+ and of the hydrogen bond distances to the two solvating water molecules and the influence of a third water molecule introduced to solvate the transferring proton will be examined later. The procedure of 3D TS determination can be visualized as having three steps. This is illustrated below for the case of 0.727 V electrode potential and the hydronium ion structure given as entry A in Table 1. Calculations are made using the MP2 method with the 6-31G** basis set. In the first step, the $OO\cdots OH_2(OH_2)_2$ and $H^+\cdots OH_2(OH_2)_2$ distances are kept fixed and the O–O distance is varied until the reaction complex has the desired EA. This is identified by the point of intersection of the plotted energies of $[OO\cdots H^+\cdots OH_2(OH_2)_2 + e^-$ (0.727 V)] and $[OO\cdots H\cdots OH_2(OH_2)_2]$ versus the O–O distance (Fig. 2a). In the second step, the $OO\cdots OH_2(OH_2)_2$ distance is maintained at a fixed value and the first step is repeated

Table 1
Internuclear distances, R (Å), and bond angles, θ (°), from MP2/6-31G** calculations for different used models of the hydronium ion hydrogen bonded with two water molecules, $H^+–OH_2(OH_2)_2$

Model	R (O–H_u)	R (O–H_s)	θ (H_sOH_u)	θ (H_sOH_s)	R ($H_s\cdots OH_2$)	θ (OH_sO)	R (O–H_a)	R (O–H_b)	θ (H_sOH_a)	θ (H_sOH_b)	θ (H_aOH_b)
A	0.966	1.040	112.9	115.6	1.438	175.4	0.965	0.964	121.1	125.9	107.4
B	0.967	1.037	112.7	115.1	1.446	175.6	0.965	0.964	121.1	125.6	107.3
C	0.969	1.024	110.5	113.7	1.529	175.9	0.964	0.964	118.2	122.1	110.9
D	0.971	1.009	108.0	112.2	1.624	168.2	0.964	0.965	115.8	118.1	112.8
E	0.974	0.989	105.2	110.8	1.774	161.3	0.964	0.965	114.1	113.7	113.0
F	0.978	0.975	100.6	108.6	1.897	151.5	0.963	0.965	112.2	106.7	110.0
G	0.982	0.972	95.5	106.4	1.985	142.3	0.963	0.965	111.1	99.5	104.1
H	0.975	0.965	110.4	105.0	2.024	152.3	0.964	0.964	87.2	92.8	103.6

Structure parameters are defined in Fig. 1.

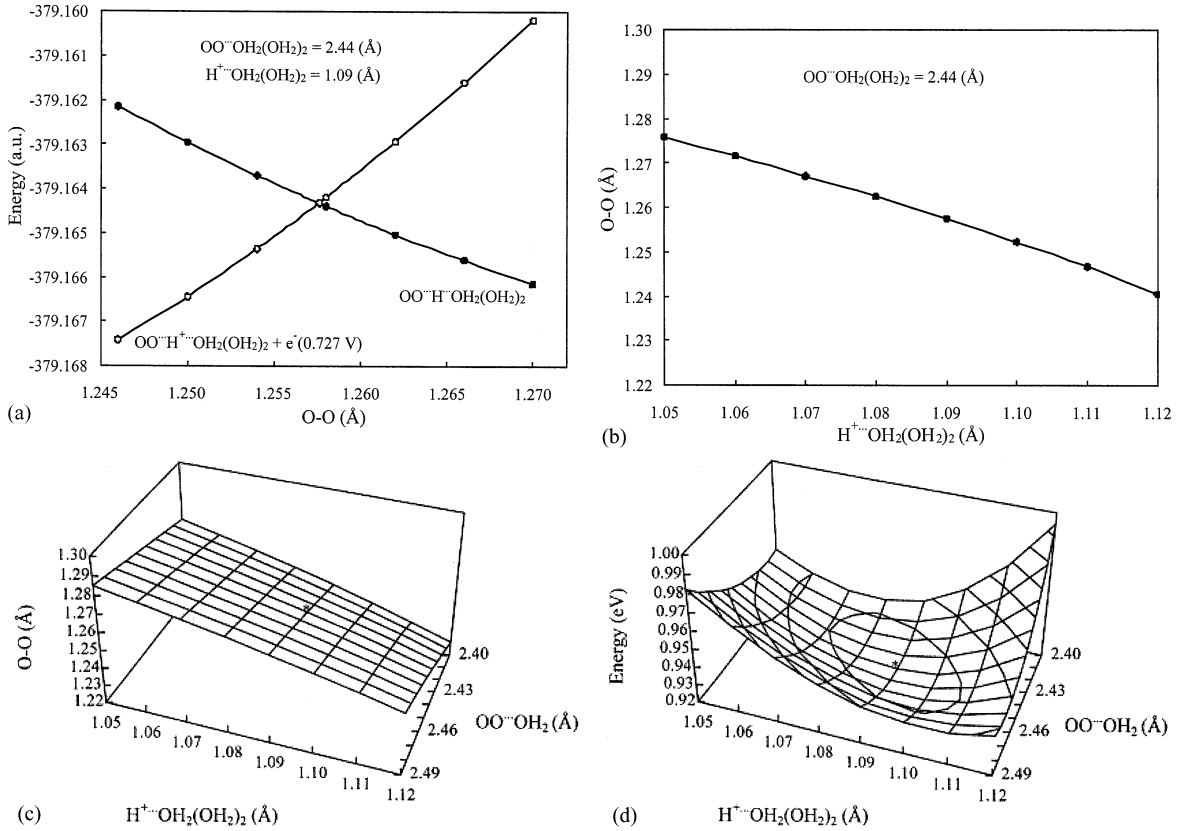

Fig. 2. Transition state determination procedure using MP2/6-31G** and the structure A for the hydronium ion exemplified for an electrode potential of 0.727 V: (a) determination of the point with EA = 5.327 eV with $OO\cdots OH_2(OH_2)_2$ and $H^+\cdots OH_2(OH_2)_2$ fixed as shown and the O–O distance varied; (b) two-dimensional, constant EA curve determined at the $OO\cdots OH_2(OH_2)_2$ distance in (a); (c) constant EA surface, with * indicating the transition state structure; and (d) the energy of the 3D, constant EA surface relative to the reduction precursor energy. The * marks the transition state.

for a number of different $H^+\cdots OH_2(OH_2)_2$ distances stepped in 0.01 Å increments to generate a constant electron-affinity curve (Fig. 2b). For the third step, the second step is repeated for a number of different $OO\cdots OH_2(OH_2)_2$ distances, also varied in 0.01 Å increments, and the results are then used to construct a 3D, constant electron-affinity hypersurface (Fig. 2c). By comparing the Born–Oppenheimer energies at structures defined by this surface with the Born–Oppenheimer energy of the reduction precursor determined with the same constraints as above, the energy surface in Fig. 2d is generated and the minimum on this surface gives the reduction activation energy (RAE). The third geometric coordinate, the O–O distance, not represented in Fig. 2d, has the same value as in Fig. 2c. The same transition state structure applies to the oxidation reaction because it is just the reverse of the reduction reaction given in Eq. (2). The oxidation activation energy (OAE), for OOH oxidation to O_2, is determined by comparing the transition state energy with the oxidation precursor energy determined with the same constraints as above. The diabatic TS determined this way is an upper limit to the adiabatic TS [36].

To evaluate the sensitivity of the activation energies to the solvation fragment structure, a number of TS determinations have been carried out for different solvating side structures (Fig. 1) with the geometric parameters given in Table 1. The MP2/6-31G** level of theory has been used. Entry A is the optimized structure of H^+–$OH_2(OH_2)_2$ and entry B is the structure of the optimized $OO\cdots H^+$–$OH_2(OH_2)_2$ system. Structure H is for the optimized $OH_2(OH_2)_2$ fragment and structure G is for the optimized $OO-H\cdots OH_2(OH_2)_2$ system. The other entries, C–F, are intermediate structures between B and G and are chosen, although somewhat arbitrarily, to have the geometric parameters between those of structures B and G.

Calculated TS structure data for 0.727 V electrode potential are given in Table 2. Respective structure data and hydrogen-bond strengths for the reduction and oxidation precursors are presented for all the solvation structures in Tables 3 and 4. The calculated energies of

precursors and transition states for structures A–H relative to the energy of optimized H^+–$OH_2(OH_2)_2$ and O_2 are graphed in Fig. 3. The transition state determined with structure C is the lowest energy one. Although structure C has been chosen arbitrarily, comparison with the other transition state energies suggests that this structure is quite close to the fully optimized transition state structure. The RAE is 0.820 eV when calculated based on the reduction precursor B and transition state C and this is 0.104 eV smaller than calculated previously using only structure A [25,26]. The OAE based on the oxidation precursor G and transition state C is 1.291 eV, which is 0.685 eV larger than the one based on the oxidation precursor and TS determined using structure A, and 0.561 eV less than when based on the oxidation precursor and TS determined using structure G. Based on these results it seems reasonable to conclude that the previously used approximation, model A, is satisfactory for the study of the O_2 reduction process, especially at small electrode potentials where distortions from the reduction precursor are limited and the calculated RAE are small. The calcu-

Table 2
Transition state internuclear distances R (Å), and activation energies, E_a (eV), for the first steps in O_2 reduction calculated with different models for hydronium ion

Model	R ($OO\cdots OH_2$)	R ($H^+\cdots OH_2$)	R ($OO\cdots H^+$)	R (O–O)	Reduction E_a	Oxidation E_a
A	2.44	1.09	1.35	1.2576	0.924	0.606
B	2.44	1.09	1.35	1.2563	0.908	0.622
C	2.46	1.08	1.38	1.2510	0.744	0.773
D	2.48	1.06	1.42	1.2484	0.579	0.952
E	2.52	1.05	1.47	1.2402	0.399	1.212
F	2.58	1.02	1.56	1.2349	0.215	1.505
G	2.75	1.00	1.75	1.2343	0.075	1.852
H	2.60	1.02	1.58	1.2276	0.150	1.920

For 0.727 V electrode potentials as based on MP2/6-31G** calculations.

Table 3
Internuclear distances, R (Å), and hydrogen bond strengths, E_{hb} (eV), for the hydrogen-bonded reduction precursors, $OO\cdots H^+-OH_2(OH_2)_2$, calculated with different models for hydronium ion

Model	R ($OO\cdots OH_2$)	R (H^+–OH_2)	R ($OO\cdots H^+$)	R (O–O)	E_{hb}
A	3.17	0.97	2.20	1.2172	0.047
B	3.17	0.97	2.20	1.2172	0.048
C	3.14	0.97	2.17	1.2170	0.056
D	3.11	0.97	2.14	1.2169	0.066
E	3.07	0.98	2.09	1.2170	0.082
F	3.04	0.98	2.06	1.2191	0.117
G	3.08	0.98	2.10	1.2261	0.174
H	2.98	0.98	2.00	1.2152	0.100

Table 4
Internuclear distances, R (Å), and hydrogen bond strengths, E_{hb} (eV), for the hydrogen-bonded oxidation precursors, $OO–H\cdots OH_2(OH_2)_2$, calculated with different models for hydronium ion

Model	R ($OO\cdots OH_2$)	R ($H\cdots OH_2$)	R (OO–H)	R (O–O)	E_{hb}
A	2.53	1.50	1.03	1.3190	1.077
B	2.54	1.51	1.03	1.3190	1.067
C	2.56	1.53	1.03	1.3198	0.997
D	2.58	1.56	1.02	1.3208	0.930
E	2.61	1.60	1.01	1.3221	0.846
F	2.61	1.60	1.01	1.3245	0.819
G	2.60	1.59	1.01	1.3292	0.834
H	2.67	1.68	0.99	1.3231	0.607

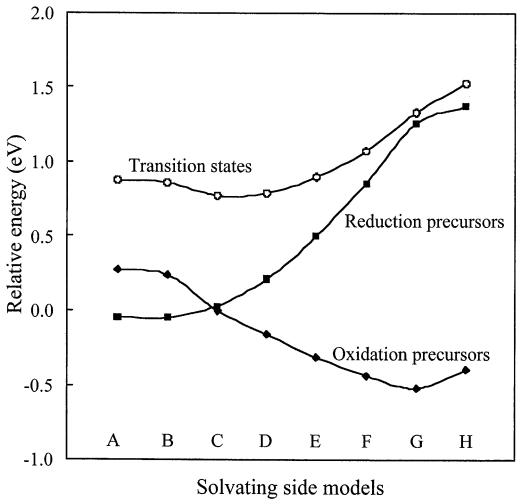

Fig. 3. Energies of 0.727 V transition states, reduction and oxidation precursors calculated with different model structures for the hydronium ion relative to the energy of optimized H^+–$OH_2(OH_2)_2$ and O_2.

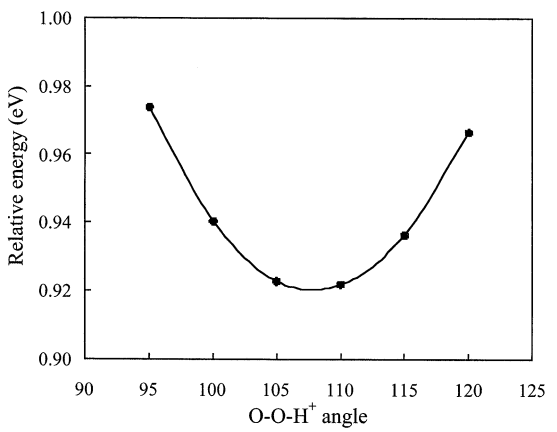

Fig. 4. Energies of the transition state for different O–O–H^+ angles relative to the reduction precursor energy.

lated OAE, based on structure A, are, however, underestimated.

Another approximation in the previous TS determinations was the setting of the O–O–H angle to the product value. To evaluate the effect of this constraint, a number of 0.727 V TS determinations at different values for the O–O–H^+ angle have been carried out at the MP2/6-31G** level using structure A. The energies of the transition states for different angles are shown in Fig. 4, and the corresponding calculated geometric parameters are given in Table 5. The assumed 104.43° angle results in an overestimation of the TS energy by only 0.003 eV, which shows that fixing the O–O–H angle along the reaction coordinate to the product value introduces small errors in calculated activation energies in this case.

3.2. Sensitivity to the calculational method and the basis set choice

Structure A for the solvated hydronium ion structure has been used in all calculations presented in this section. Transition state structures and activation energies at several potentials determined as presented above are given in Table 6 and the precursor structures for O_2 reduction and OOH oxidation are given in Tables 7 and 8. The electrode potential dependencies of the RAE and OAE using the 6-31G** and 6-31 + G** basis sets and various calculational approaches are graphed in Figs. 5 and 6, respectively. The trend lines are similar in shape, so a single potential, 0.727 V, is chosen for the comparison. The RAE calculated at the HF/6-31G** level is the highest, 1.338 eV, and adding diffuse functions lowers it by 0.251 eV. The MP2 energies are next highest, 0.924 eV, and adding diffuse functions lowers the RAE by 0.395 eV. The RAE at the B3LYP/6-31G** level is 0.422 eV, actually 0.107 eV smaller than the diffuse function MP2 value. Finally, the diffuse function B3LYP value for the RAE is the lowest, 0.278 eV lower than the 6-31G** result. According to the

Table 5
Internuclear distances, R (Å), for transition states calculated at different values for the O–O–H^+ angle, θ (°), and their energies (eV) compared to reduction precursor

θ (O–O–H^+)	R (OO···OH_2)	R (H^+···OH_2)	R (OO···OH^+)	R (O–O)	Relative energy (eV)
95	2.46	1.08	1.38	1.2620	0.974
100	2.44	1.08	1.36	1.2599	0.940
105	2.44	1.09	1.35	1.2579	0.923
110	2.43	1.09	1.34	1.2591	0.922
115	2.43	1.10	1.33	1.2582	0.936
120	2.42	1.11	1.31	1.2556	0.966

The electrode potentials 0.727 eV.

Table 6
Transition state internuclear distances R (Å), and activation energies, E_a (eV), for the one-electron O_2 reduction and OOH oxidation calculated with different methods at different electrode potentials (V)

Method	Electrode potential	R ($OO\cdots OH_2$)	R ($H^+\cdots OH_2$)	R ($OO\cdots H^+$)	R (O–O)	Reduction E_a	Oxidation E_a
HF/6-31G**	0.300	2.42	1.06	1.36	1.2569	1.049	0.871
	0.727	2.40	1.11	1.29	1.2603	1.338	0.733
	1.250	2.38	1.17	1.21	1.2628	1.701	0.573
	2.000	2.39	1.27	1.12	1.2702	2.221	0.344
HF/6-31+G**	0.300	2.47	1.03	1.44	1.2522	0.804	0.978
	0.727	2.42	1.07	1.35	1.2585	1.087	0.834
	1.250	2.39	1.13	1.26	1.2634	1.452	0.676
	2.000	2.38	1.23	1.15	1.2661	1.975	0.449
B3LYP/6-31G**	0.300	2.58	1.02	1.56	1.2605	0.232	0.985
	0.727	2.50	1.05	1.45	1.2740	0.422	0.748
	1.250	2.45	1.10	1.35	1.2906	0.714	0.518
	2.000	2.42	1.20	1.22	1.2995	1.212	0.265
B3LYP/6-31+G**	0.300	2.80	0.99	1.81	1.2334	0.039	1.426
	0.727	2.66	1.01	1.65	1.2513	0.144	1.104
	1.250	2.54	1.04	1.50	1.2728	0.352	0.788
	2.000	2.44	1.11	1.33	1.2942	0.776	0.462
MP2/6-31G**	0.300	2.48	1.06	1.42	1.2482	0.662	0.771
	0.727	2.44	1.09	1.35	1.2576	0.924	0.606
	1.250	2.41	1.14	1.27	1.2656	1.277	0.436
	2.000	2.41	1.23	1.18	1.2789	1.824	0.233
MP2/6-31+G**	0.300	2.58	1.01	1.57	1.2407	0.314	1.048
	0.727	2.51	1.04	1.47	1.2489	0.529	0.836
	1.250	2.45	1.08	1.37	1.2595	0.842	0.626
	2.000	2.41	1.16	1.25	1.2712	1.353	0.387
MP2/6-31G	0.727	2.51	1.08	1.43	1.3373	1.072	0.422
MP2/6-31G*	0.727	2.46	1.10	1.36	1.2602	0.984	0.620
MP2/6-31++G**	0.727	2.51	1.04	1.47	1.2487	0.526	0.838
MP2/6-31+G**	0.727	2.48	1.04	1.44	1.2372	0.556	0.838
MP2/6-311++G**	0.727	2.48	1.04	1.44	1.2371	0.554	0.839
MP2/6-311+G(2d,p)	0.727	2.52	1.04	1.48	1.2398	0.455	0.872
QCISD/6-31G**	0.727	2.46	1.07	1.39	1.3076	0.690	0.706

literature, HF overestimates activation energies for simple hydrogen transfer reactions [37], and DFT underestimates them [37–39]. The MP2 and QCISD results are expected to be relatively accurate.

Regarding O_2 reduction, it is believed that the first step, OOH(ads) formation, Eq. (2), is rate limiting over the three low-index Pt surfaces and, from the temperature dependence of exchange currents extrapolated from Tafel plots in the double layer region, an activation enthalpy of 0.44 eV has been determined for this at the oxygen reduction reversible potential (1.23 V) in 0.05 M sulfuric acid [12]. Calculations using the MP2/6-31G** approach for O_2 reduction when end-on bonded to a Pt atom in a bent structure yielded an activation energy of 0.43 eV at 1.23 V for the first step [27]. The near match with the experimental activation energy (0.44 eV) must be regarded as fortuitous because of the approximations in the theoretical model. From Table 6, the activation energy for first step in the uncatalyzed reduction at 1.23 V is 0.92 eV, much higher than the calculated platinum-catalyzed result in Ref. [27]. An experimental value for the uncatalyzed activation energy is not available, but over weakly interacting mercury [28] and diamond [40] electrodes the overpotential for oxygen reduction is higher than it is over platinum electrodes, and this means that the activation energy is also higher. The calculated RAEs are consistent with these experimental findings.

The dependence on basis set within the MP2 approach is the next topic. The split valence double-ζ 6-31G basis set gives the highest RAE of the basis sets investigated, 1.072 eV. This is despite a weak O_2 bond with a length of 1.343 Å. Addition of the d set of orbitals to oxygen in 6-31G* improves the description of the O_2 molecule, the bond length being 1.247 Å, and the calculated RAE is reduced by 0.088 eV. Addition of

p orbitals to the hydrogen atoms further reduces the activation energy by only 0.060 eV. Addition of a set of diffuse function on oxygen has a large effect, yielding a RAE with the 6-31 + G** basis of 0.529 eV, which is 0.395 eV smaller than that calculated with 6-31G**. Additional diffuse functions on hydrogen atoms, in the 6-31 + + G** basis set, have little effect, lowering the RAE by only 0.003 eV.

A split valence triple-ζ basis set 6-311 + G** instead of a double-ζ, increases the RAE by 0.027 eV and adding a second set of d functions for oxygen, 6-311 + G(2d,p), decreases it by 0.101 eV. As expected, by using a larger basis set, the reactant EA in the reduction precursor structure is increased, so the reaction center requires smaller distortions to reach the desired EA and this decreases the calculated RAE. In contrast, using a larger basis set in calculating OAE results in an increase because this stabilizes the neutral oxidation precursor more than its oxidized form. It is interesting to note that the calculated MP2/6-311 + G(2d,p) and B3LYP/6-31G** activation energy values are very close, and this shows that the latter method may be useful for oxygen reduction studies.

The calculated activation energies are all sensitive to the addition of diffuse functions on oxygen. Over the electrode potential range investigated, between 0.3 and 2.0 V, the RAEs are decreased on average by 0.412 eV using MP2, by 0.317 eV using B3LYP, and by 0.248 eV using HF. The OAEs are increased on average by 0.213 eV at the MP2 level, by 0.316 eV at the B3LYP level, and by 0.104 eV at the HF level of calculation. The changes are different for the reduction and oxidation because the diffuse functions change also the relative energies of the reduction and oxidation precursors.

Table 7
Internuclear distances, R (Å), and hydrogen bond strengths, E_{hb} (eV), for the hydrogen-bonded reduction precursors, $OO\cdots H^+$ $-OH_2(OH_2)_2$, calculated with different methods

Method	R ($OO\cdots OH_2$)	R ($H^+\cdots OH_2$)	R ($OO\cdots OH^+$)	R (O–O)	E_{hb}
HF/6-31G**	3.21	0.95	2.26	1.1692	0.064
HF/6-31 + G**	3.27	0.95	2.32	1.1705	0.045
B3LYP/6-31G**	3.00	0.97	2.03	1.2162	0.127
B3LYP/6-31 + G**	3.05	0.97	2.08	1.2168	0.074
MP2/6-31G	3.49	0.98	2.51	1.3067	0.005
MP2/6-31G*	3.16	0.98	2.18	1.2171	0.052
MP2/6-31G**	3.17	0.97	2.20	1.2172	0.047
MP2/6-31 + G**	3.21	0.97	2.24	1.2211	0.041
MP2/6-31 + + G**	3.21	0.97	2.24	1.2211	0.045
MP2/6-311 + G**	3.20	0.97	2.23	1.2077	0.050
MP2/6-311 + + G**	3.20	0.97	2.23	1.2077	0.054
MP2/6-311 + G(2d,p)	3.17	0.97	2.20	1.2144	0.055
QCISD/6-31G**	3.05	0.97	2.08	1.2277	0.122

Table 8
Internuclear distances, R (Å), and hydrogen bond strengths, E_{hb} (eV), for the hydrogen-bonded oxidation precursors, $OO-H\cdots OH_2(OH_2)_2$, calculated with different methods

Method	R ($OO\cdots OH_2$)	R ($H\cdots OH_2$)	R (OO–H)	R (O–O)	E_{hb}
HF/6-31G**	2.62	1.64	0.98	1.3078	0.838
HF/6-31 + G**	2.66	1.68	0.98	1.3077	0.695
B3LYP/6-31G**	2.53	1.49	1.04	1.3342	1.127
B3LYP/6-31 + G**	2.55	1.52	1.03	1.3360	0.885
MP2/6-31G	2.54	1.48	1.06	1.3739	1.245
MP2/6-31G*	2.57	1.54	1.03	1.3194	1.072
MP2/6-31G**	2.53	1.50	1.03	1.3190	1.077
MP2/6-31 + G**	2.56	1.53	1.03	1.3232	0.894
MP2/6-31 + + G**	2.56	1.53	1.03	1.3233	0.894
MP2/6-311 + G**	2.55	1.53	1.02	1.3081	0.873
MP2/6-311 + + G**	2.55	1.53	1.02	1.3081	0.878
MP2/6-311 + G(2d,p)	2.56	1.53	1.03	1.3141	0.856
QCISD/6-31G**	2.56	1.55	1.01	1.3519	1.000

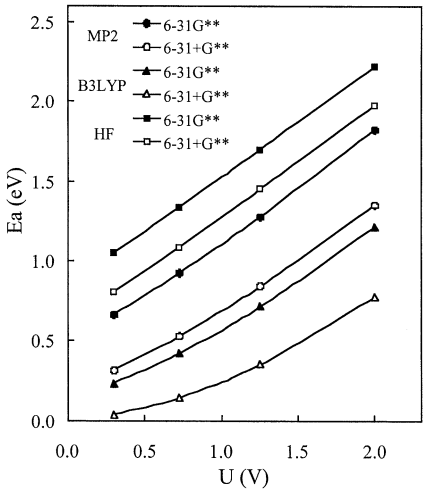

Fig. 5. Activation energies for the one-electron oxygen reduction step function of the electrode potential, determined at different levels of calculation.

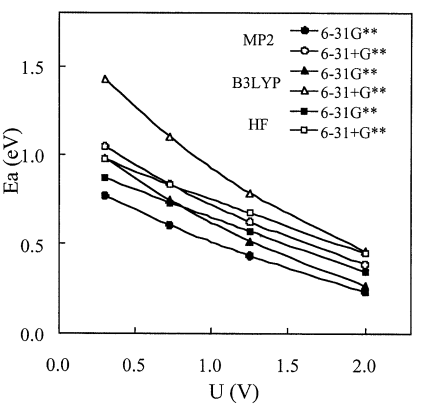

Fig. 6. Activation energies for the one-electron hydroperoxyl oxidation step function of the electrode potential, determined at different levels of calculation.

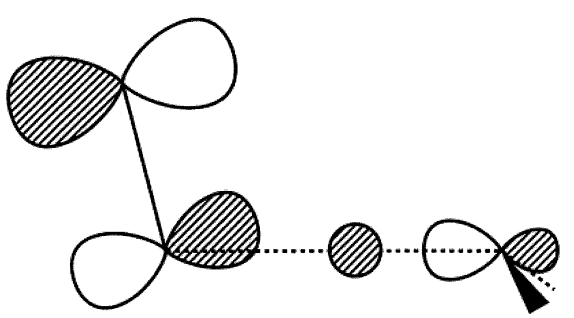

Fig. 7. Orbital that accepts electron at transition state of first step in oxygen reduction (MP2/6-31G** level of calculation used).

A comparative analysis of the molecular orbital basis sets used in the MP2/6-31G** and MP2/6-31 + G** calculations is considered below (with the 6-31 + G** results in square brackets). The empty, degenerate, β-spin π* orbitals of the triplet oxygen in its ground state are located at 2.665 [2.010] eV. Due to the electric field of the hydronium ion, these orbitals split and became more stable at −1.025 [−1.582] and −0.761 [−1.371] eV in the hydrogen-bonded reduction precursor. Because of the C_s symmetry of the reaction center, one of these orbitals is pure π*, perpendicular to the symmetry plane, while the other is in-plane and has a weak bonding overlap with the transferring proton. At the 0.727 V TS, before the electron transfers, these orbitals became even further stabilized at −2.840 [−2.783] eV for the pure π* and at −2.736 [−2.774] eV for the in-plane one. The electron transfers to the in-plane orbital, Fig. 7, which moves, upon occupation, to −6.957 [−6.935] eV as the empty pure π* moves up to 7.817 [5.227]. Because the orbital that accepts the electron is mostly located on O_2, the bond order of O_2 decreases from 2 to 3/2 which has the effect of increasing the O–O bond length while the $OO\cdots H^+$ distance decreases. When the electron transfers, the calculated net Mulliken charge on the OO fragment decreases from 0.067 [0.055] to −0.807 [−0.853] and for the hydronium ion from 0.783 [0.868] to 0.699 [0.834]. At this moment, the reaction center is an ion pair consisting of O_2^- and solvated H^+–OH_2 and the energy drops as it relaxes to the $OOH\cdots OH_2(OH_2)_2$ product. Thus the transition state coincides with the electron transfer state.

The reaction center at the 0.727 V TS has an EA of 5.327 eV. The EA for the separated fragments, with the same geometries as in the TS, are −1.275 [−0.278] eV for OO and 1.287 [2.176] eV for the solvated hydronium ion, $H^+\cdots OH_2(OH_2)_2$. The EA for O_2 is negative because its bond has stretched only ∼0.03 Å from equilibrium and because of theoretical model limitations. The EA for both fragments are more positive when calculated with the larger 6-31 + G** basis set with diffuse functions, although when together in the TS they have an EA of 5.327 eV. This finding is understood by considering the structures of the precursors and the transition states. As seen in Table 7, the presence of diffuse functions has a small effect on the precursor bond lengths. However, at the TS, for 6-31G** calculations, the $OO\cdots H^+$ bond is shorter at 1.35 Å and $H^+\cdots OH_2$ is longer at 1.09 Å compared with the values of 1.47 and 1.04 Å, respectively, when 6-31 + G** is used (Table 6). The reaction must proceed further to achieve the desired EA when the diffuse functions are absent, and this also increases the activation energy. For both basis sets, the hydronium ion electric field increases the EA of the OO fragment and plays a significant role in activating O_2 reduction in acid electrolytes.

3.3. Effect of enhancing the solvated hydronium ion model

Another aspect to explore is the effect of additional solvation. This is done by using a $H^+OH_2(OH_2)_3$ model for the hydronium ion. As was discussed elsewhere [26], the experimental proton solvation energy of 11.305 eV [35] is well reproduced by a $H^+OH_2(OH_2)_3$ model, which predicts a value of 11.61 eV at the MP2/6-31G** level of calculation. For this study, the additional water molecule is hydrogen bonded to the transferring proton in the reduction precursor, optimized to be 2.673 Å away, when constrained to be in the system's plane of symmetry (Fig. 1), thus retaining the C_s symmetry. The water molecule is kept fixed relative to the transferring proton's position along the reaction coordinate. In this case the calculated RAE at the 0.727 V electrode potential is 1.203 [0.736] eV at the MP2/6-31G** [MP2/6-31 + G**] level, which is 0.279 [0.209] eV greater than before. The increase is understandable because the positively charged reactants are stabilized more than the neutral products when more water lone-pairs are coordinated to it: the increased stabilization of the reaction center decreases its EA and a higher thermal activation is required to reach the structures with the desired EA. It is interesting to note that, because RAE are decreased on average by 0.268 eV by adding diffuse functions, the net effect of improving the model by both increasing the basis set and enhancing the solvation model is small.

3.4. Potential dependence of the activation energies and the Butler–Volmer equation

The well-known Butler–Volmer equation predicts the relationship between the current density, j, and the overpotential, $\eta = U - U_{rev}$, to be:

$$j = j_0(e^{\alpha_0 F\eta/RT} - e^{-\beta_0 F\eta/RT}) \quad (9)$$

where j_0 is the exchange current, α_0 the anodic transfer coefficient, β_0 the cathodic transfer coefficient, and F the Faraday constant. Eq. (9) comes from absolute rate theory and assumes that the preexponential factor is independent of overpotential and that activation free energy, ΔG^*, has a linear dependence on overpotential around the reversible potential, U_{rev} [41]:

$$\Delta G^*_{ox}(U) = \Delta G^*(U_{rev}) - \alpha_o F\eta = \Delta G^*(U_{rev}) - \alpha_o F(U - U_{rev}) \quad (10)$$

$$\Delta G^*_{rd}(U) = \Delta G^*(U_{rev}) + \beta_o F\eta = \Delta G^*(U_{rev}) + \beta_o F(U - U_{rev}) \quad (11)$$

When the potential energy surfaces of the reactants and products are not dependent on the overpotential, which is true in this outer-Helmholtz-plane study, and is generally expected for outer-sphere reactions, the transfer coefficients, known also as symmetry factors, are then related through $\alpha_0 + \beta_0 = 1$.

On the assumptions that: (i) the activation enthalpy differs insignificantly from the activation energy E_a at a given temperature, about 1 J/mol [42]; and (ii) the entropy of activation is nearly potential independent, which is supported by the similarity of transition state structures in Table 6, then $\alpha(U)$ and $\beta(U)$ can be estimated from Eqs. (10) and (11) as follows:

$$\alpha(U) = -1/F(\partial G^*_{ox}/\partial U) \cong -1/F(\partial E_a/U) \quad (12)$$

$$\beta(U) = 1/F(\partial \Delta G^*_{rd}/\partial U) \cong 1/F(\partial E_a/\partial U) \quad (13)$$

Thus, over the 0.3–2.0 V range studied, $\alpha(U)$ and $\beta(U)$ are approximated as the slopes of the curves $E_a(U)$ represented in Figs. 5 and 6. Using a second-order polynomial fitting of these curves, for the MP2/6-31G** [MP2/6-31 + G**] method, $\alpha(U) = 0.431 - 0.100 \cdot U/V$ [$\alpha(U) = 0.565 - 0.154 \cdot U/V$] and $\beta(U) = 0.569 + 0.100 \cdot U/V$ [$\beta(U) = 0.435 + 0.154 \cdot U/V$]. These fits provide a way to calculate the transfer coefficients α_0 and β_0 from Eqs. (10) and (11) when the reversible potential is known. In the present model the reversible potential can be determined based on the relative energies of the hydrogen-bonded precursors and this is 0.409 [1.034] V. At this potential, $\alpha_0 = 0.390$ [0.406] and $\beta_0 = 0.610$ [0.594]. Although close to 0.5, the calculated values for α_0 and β_0 are not equal because the 3D potential energy surfaces are asymmetric near the calculated TS at this potential. Savéant also calculated potential-dependent symmetry factors for the case of dissociative reduction of alkyl halides [43]. However, that model had only two independent variables: a Marcus–Hush-type solvent reorganization energy [44,45], and the carbon–halogen Morse potential curve.

Phenomenologically, $\beta(U)$ will increase from a value of 0 at a potential where TS has the structure of the reduction precursor corresponding to a very early TS for the reduction process, to a value of one at a potential where TS has the structure of the oxidation precursor, corresponding to a very late TS for the reduction process [46]. From the calculated reduction precursor's EA and oxidation precursor's IP, using MP2/6-31G** [MP2/6-31 + G**] calculations, $\beta(U)$ is 0 at -1.866 [-1.108] V and becomes 1 at 3.506 [4.016] V. These potential values are outside of the range of the above polynomial fit.

4. Conclusions

For the first one-electron step in the uncatalyzed oxygen reduction, the electron transfer state is found to occur at the transition state over the 0.3–2.0 V potential range. The transition state is primarily sensitive to three structure variables: O–O, $OO\cdots OH_2(OH_2)_2$, and H^+–$OH_2(OH_2)_2$ distances, with the optimal $OH_2(OH_2)_2$

structure being close to that of the optimized $H^+OH_2(OH_2)_2$ ion. MP2/6-31 + G** and B3LYP/6-31G** yield similar results in this study. Two modifications to the model: (a) addition of a water molecule coordinated to the transferring proton and (b) extending the basis set to include diffuse functions, have opposite effects on the calculated reduction activation energy. It is concluded that, considering the opposing influence of these model improvements, a H^+–$OH_2(OH_2)_2$ model for the hydronium ion and the MP2/6-31G** calculational approach may be considered adequate for studying potential-dependent trends in the activation energies for steps in the outer-sphere reduction of oxygen.

Acknowledgements

The US Army Research Office partially supported the work through grant no. DAAD 19-99-1-0253.

References

[1] (a) S. Mukerjee, S. Srinivasan, M.P. Soriaga, J. McBreen, J. Phys. Chem. 99 (1995) 4577;
(b) S. Mukerjee, S. Srinivasan, M.P. Soriaga, J. McBreen, J. Electrochem. Soc. 142 (1995) 1409.
[2] (a) S. Strbac, R.R. Adzic, Electrochim. Acta 41 (1996) 2903;
(b) S. Strbac, R. Adzic, Electroanal. Chem. 403 (1996) 169.
[3] S. Trasatti, in: A. Wieckowski (Ed.), Interfacial Electrochemistry: Theory, Experiment and Applications, Marcel Dekker, New York, 1999, p. 769.
[4] S. Gupta, D. Tryk, S.K. Zecevic, W. Aldred, D. Guo, R.F. Savinell, J. Appl. Electrochem. 28 (1998) 673.
[5] S.L. Gojkovic, S. Gupta, R.F. Savinell, J. Electroanal. Chem. 462 (1999) 63.
[6] O. El Mouahid, A. Rakotondrainibe, P. Crouigneau, J.M. Leger, C. Lamy, J. Electroanal. Chem. 455 (1998) 209.
[7] G. Faubert, R. Cote, D. Guay, J.P. Dodelet, G. Denes, P. Bertrand, Electrochim. Acta 43 (1998) 341.
[8] (a) P. Gouerec, M. Savy, J. Riga, Electrochim. Acta 43 (1998) 743;
(b) P. Gouerec, M. Savy, Electrochim. Acta 44 (1999) 2653.
[9] J.O'M. Bockris, S.U.M. Khan, Surface Electrochemistry, Plenum, New York, 1993 (Ch. 3).
[10] F.C. Anson, C. Shi, B. Steiger, Acc. Chem. Res. 30 (1997) 437.
[11] R. Adzic, in: J. Lipkowski, P.N. Ross (Eds.), Electrocatalysis, Wiley, New York, 1998 (p. 197).
[12] N.M. Markovic, P.N. Ross, in: A. Wieckowski (Ed.), Interfacial Electrochemistry: Theory, Experiment and Applications, Marcel Dekker, New York, 1999, p. 821.
[13] (a) M.T.M. Koper, G.A. Voth, Chem. Phys. Lett. 282 (1998) 100;
(b) M.T.M. Koper, G.A. Voth, J. Chem Phys. 109 (1998) 1991.
[14] M.T. Koper, W. Schmickler, in: J. Lipkowski, P.N. Ross (Eds.), Electrocatalysis, Wiley, New York, 1998, p. 291.
[15] S. Walbran, A. Mazzolo, J.W. Halley, D.L. Price, J. Chem. Phys. 109 (1998) 8076.
[16] J.W. Halley, S. Walbran, D.L. Price, in: A. Wieckowski (Ed.), Interfacial Electrochemistry: Theory, Experiment and Applications, Marcel Dekker, New York, 1999, p. 1.
[17] E. Spohr, Electrochim. Acta 44 (1999) 1697.
[18] J.O'M. Bockris, R. Abdu, J. Electroanal. Chem. 448 (1998) 189.
[19] C.F. Zinola, A.J. Arvia, G.L. Estiu, E.A. Castro, J. Phys. Chem. 98 (1994) 7566.
[20] S.P. Mehandru, A.B. Anderson, Surf. Sci. 216 (1989) 105.
[21] A.B. Anderson, Proc. Electrochem. Soc. 92 (1992) 434.
[22] J.H. Zagal, Coord. Chem. Rev. 119 (1992) 89.
[23] R.W. Gurney, Proc. R. Soc. A 134 (1931) 137.
[24] A.B. Anderson, D.B. Kang, J. Phys. Chem. A 102 (1998) 5993.
[25] A.B. Anderson, T.V. Albu, Electrochem. Commun. 1 (1999) 203.
[26] A.B. Anderson, T.V. Albu, J. Am. Chem. Soc. 121 (1999) 11 855.
[27] A.B. Anderson, T.V. Albu, Electrochem. Soc. 147 (2000) 4229.
[28] J.P. Hoare, The Electrochemistry of Oxygen, Interscience, New York, 1968 (p. 163).
[29] N.M. Markovic, H.A. Gasteiger, P.N. Ross, J. Phys. Chem. 99 (1995) 3411.
[30] (a) A.M. Kuznetsov, W. Lorenz, Chem. Phys. 185 (1994) 333;
(b) A.M. Kuznetsov, W. Lorenz, Chem. Phys. 214 (1997) 243.
[31] J. Lukowczyk, C. Engler, Z. Phys. Chem. 203 (1998) 159.
[32] A. Hofmann, C. Engler, Z. Phys. Chem. 210 (1999) 95.
[33] W. Lorenz, J. Phys. Chem. 95 (1991) 10 566.
[34] M.J. Frisch, G.W. Trucks, H.B. Schlegel, G.E. Scuseria, M.A. Robb, J.R. Cheeseman, V.G. Zakrzewski, J.A. Montgomery, R.E. Stratmann, J.C. Burant, S. Dapprich, J.M. Millam, A.D. Daniels, K.N. Kudin, M.C. Strain, O. Farkas, J. Tomasi, V. Barone, M. Cossi, R. Cammi, B. Mennucci, C. Pomelli, C. Adamo, S. Clifford, J. Ochterski, G.A. Petersson, P.Y. Ayala, Q. Cui, K. Morokuma, D.K. Malick, A.D. Rabuck, K. Raghavachari, J.B. Foresman, J. Cioslowski, J.V. Oritz, A.G. Baboul, B. Stefanov, G. Liu, A. Liashenko, P. Piskorz, I. Komaromi, R. Gomperts, R.L. Martin, D.J. Fox, T. Keith, M.A. Al-Laham, C.Y. Peng, A. Nanayakkara, C. Gonzalez, M. Challacombe, P.M.W. Gill, B. Johnson, W. Chen, M.W. Wong, J.L. Andres, M. Head-Gordon, E.S. Replogle, J.A. Pople, GAUSSIAN-98 (Revision a.7), Gaussian Inc., Pittsburgh, PA, 1998.
[35] J.O'M. Bockris, S.U.M. Khan, Surface Electrochemistry, Plenum, New York, 1993 (Section 5.3).
[36] W. Schmickler, Interfacial Electrochemistry, Oxford University Press, New York, 1996.
[37] L. Ackerman, J.D. Gale, C.R.A. Catlow, J. Phys. Chem. B 101 (1997) 10 028.
[38] M. Pavese, S. Chawla, D. Lu, J. Lobaugh, G.A. Voth, J. Chem. Phys. 107 (1997) 7428.
[39] M.T. Nguyen, S. Creve, L.G. Vanquickenborne, J. Phys. Chem. 100 (1996) 18 422.

[40] T. Yano, E. Popa, D.A. Tryk, K. Hashimoto, A. Fujishima, J. Electrochem. Soc. 146 (1999) 1081.
[41] R.J. Miller, G.L. McLendon, A.J. Nozik, W. Schmickler, F. Willig, Surface Electron-Transfer Processes, VCH, New York, 1995.
[42] J.O'M. Bockris, S.U.M. Khan, Surface Electrochemistry, Plenum, New York, 1993 (Ch. 3, p. 246).
[43] (a) J.-M. Savéant, J. Am. Chem. Soc. 109 (1987) 6788; (b) J.-M. Savéant, J. Am. Chem. Soc. 114 (1992) 10 595.
[44] R.A. Marcus, N. Sutin, Biochim. Biophys. Acta 811 (1985) 265.
[45] N.S. Hush, J. Electroanal. Chem. 470 (1999) 170.
[46] A.M. Kuznetsov, J. Ulstrup, Electron Transfer in Chemistry and Biology. An Introduction to the Theory, Wiley, New York, 1999 (p. 102).